The probability of first excursion failure P_k of the kth structural member follows from Eq. (3) as

$$P_k = \int_{-\infty}^{\infty} (1 - \exp\{-\exp[-\sigma_k(x - \mu_k)]\}) f_k(x) dx \qquad (5)$$

where $f_k(x)$ is the probability density of the ultimate strength of the kth member, and σ_k and μ_k are the associated distribution parameter which can easily be estimated from Fig. 2.

It follows from Eq. (1) or Eq. (2) that the computation of 27 samples of maximum stress response Z_j; $j = 1,2,\ldots, 27$, for each structural member requires neither heavy computational effort nor excessive storage in computer. In fact, using the fast Fourier transform, Z_j can easily be computed [Eq. (2)]. Therefore, the cost involved in computing the structural reliability, Eq. (5), as well as redesign of spacecraft structures is within practical limitation.

Since it is not difficult to compute structural reliability [Eq. (5)], one can proceed to perform the reliability-based optimum design of spacecraft structures[12]; minimize the structural weight subject to the constraint that the overall probability of failure of the spacecraft structures should be less than certain value p_g. The feasibility of incorporating the notion of reliability in optimum design is another advantage of the current approach. It should be mentioned that much research work remains to be done before the nonstationary random vibration approach can be incorporated in optimum structural design.

Conclusion

Under nonstationary random excitations resulting from booster engine shutdown, a direct statistical analysis of spacecraft maximum response is performed and the spacecraft structural reliability is obtained. It is found that the Gumbel Type I asymptotic distribution of maximum values provides a reasonably good statistical model for spacecraft maximum responses. The current approach makes it possible to perform the reliability-based optimum design of spacecraft structures.

References

[1] Marx, M. H. et al., "Evaluation of Techniques for Estimating Titan III-C Flight Loads," AIAA Paper 70-485, Los Angeles, Calif., 1970.

[2] "Titan Launch Vehicle-Stage I Thrust Transient Data Book," MCR-70-8, Jan. 1970, Martin Marietta Aerospace Group, Denver Div., Denver, Colo.

[3] Lin, Y. K., *Probabilistic Theory of Structural Dynamics*, McGraw-Hill, New York, 1967.

[4] Drenick, R. F., "On the Model-Free Design of a Seismic Structure," *Journal of the Engineering Mechanics Division*, ASCE, Vol. 96, No. EM4, Aug. 1970, pp. 483–493.

[5] Shinozuka, M., "Maximum Structural Response to Seismic Excitations," *Journal of the Engineering Mechanics Division*, ASCE, Vol, 96, No. EM5, Oct. 1970, pp. 729–738.

[6] Yang, J.-N. and Heer, E., "On Maximum Dynamic Response and Proof Testing," *Journal of the Engineering Mechanics Division*, ASEC, Vol. 97, No. EM4, Aug. 1971, pp. 1307–1313.

[7] Shinozuka, M. and Yang, J.-N., "Peak Structural Response to Non-stationary Random Excitation," *The Journal of Sound and Vibration*, Vol. 16, No. 4, 1971, pp. 505–517.

[8] Gumbel, E. J., *Statistics of Extremes*, Columbia University Press, New York, 1958.

[9] Yang, J.-N., "On the Statistical Distribution of Spacecraft Maximum Structural Response," *Quarterly Technical Review*, Jet Propulsion Laboratory, Vol. 1, No. 2, July 1971, pp. 71–79.

[10] Lindgren, B. W., *Statistical Theory*, Macmillan, New York, 1962, p. 300.

[11] Wirsching, P. H. and Yao, J. T. P., "Distribution of Response to Simulated Earthquakes," *Journal of the Engineering Mechanics Division*, ASCE, Vol. 96, No. EM4, Aug. 1970, pp. 515–519.

[12] Heer, E. and Yang, J.-N., "Optimization of Structures Based on Fracture Mechanics and Reliability Criteria," *AIAA Journal*, Vol. 9, No 4, April 1971, pp. 621–628.

Directional Behavior of Thermal Emission from a Rough Lunar Surface

A. S. ADORJAN*

General Electric Company, Houston, Texas

Introduction

EARTH-BASED measurements of the infrared emission from the lunar surface revealed significant directionality effects. Temperatures along the lunar equator do not follow the Lambertian behavior, i.e., a variation according to the $\cos^{1/4}\theta$ relation. (θ is the angle measured from the subsolar point.) Pettit and Nicholson[1] suggested a $\cos^{1/6}\theta$ law to describe the directionality. Experiments and studies by Shorthill and Saari[2] indicate that the latter relation does not hold for low solar elevation angles, where the actual temperature is higher than the one predicted by the $\cos^{1/6}\theta$ relation.

The directionality of the emission can easily be explained qualitatively by the topographical roughness of the lunar surface. Surface features such as craters, hills, rilles, etc. are hotter on their sunlit sides than on the shadowed sides. Viewing these features from different directions, the emission sensed will vary according to the proportions of hotter and colder regions within the field of view. The present study postulates a rough surface, where the roughness is characterized by a crater field on a plain surface. The contour of the craters is assumed to be spherical; consequently the thermal emission can be determined based on the temperature distribution obtained analytically by Adorjan.[3] By integrating the radiosities of both the craters and plain surfaces over a control area, and for given solar elevation and observation angles, the brightness temperatures can be determined. The actual location of the individual craters within the control area is not significant, only their aspect ratios and cumulative sizes, i.e., the fraction of the control area occupied by craters with a given aspect ratio.

Analysis

Figure 1 shows the model of the lunar crater used in the analysis. The control area, which is located in the region of the lunar equator, is a flat surface, square in shape. The length of the side of the square is L. The control area contains one or more craters. The craters are characterized by their diameters, D, and by their aspect ratios, a. (When a single crater is sensed, the control surface is circular, corresponding to the area of opening of the crater.)

By using the simplification of earlier crater analysis (Ref. 3) it is assumed that both the absorptivity and emissivity of the

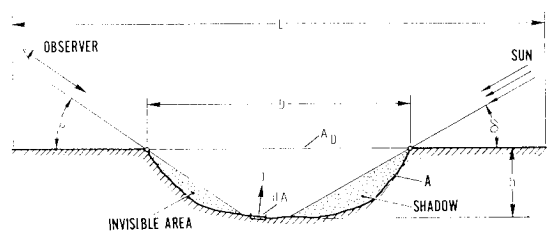

Fig. 1 Model of rough lunar surface.

Received May 19, 1971; revision received September 27, 1971. Study supported by NASA Manned Spacecraft Center under Contract NAS 9-10230.

Index categories: Radiation and Radiative Heat Transfer; Thermal Surface Properties; Thermal Modeling and Experimental Thermal Simulation.

* Consulting Engineer. Member AIAA.

lunar soil are equal to unity. Then the radiosity of the control surface can be written as

$$J = \left(1 - \sum_{i=1}^{n} A_{Dn}\right)(S \sin\delta + q_s) + \sum_{i=1}^{n} \int_{A_n} J_{cn} dA_n \qquad (1)$$

where S is the solar constant, δ is the solar elevation angle, b_s is a source term, accounting for the thermal inertia (as defined in Ref. 3). A_D and A are the opening area and surface area of the crater, respectively. For convenience the geometrical dimensions can be normalized without loss of generality. By taking $L^* = 1$, $D^* = D/L$ and $h^* = h/L$, A_D and A are calculated from these quantities. J_c is the radiosity of the crater surface. By selecting a spherical surface for the crater geometry, according to Ref. 3 the crater radiosity is

$$J_c = S(\mathbf{s} \cdot \mathbf{n}) + (4/a^2 + 1)q_s + (S \sin\delta)/(a^2/4 + 1) \qquad (2)$$

where $a = D/h$, the aspect ratio of the crater and $\mathbf{s} \cdot \mathbf{n}$ is the scalar product of the solar ray unit vector and crater surface unit normal vector, respectively.

The first term in Eq. (1) accounts for the emission of the flat surface and the second term is the summation of the emissions of the individual craters. The term $S \sin\delta + q_s$ is a simplified surface temperature vs lunation relation as defined in Ref. 3. In the present study, the thermal inertia term, q_s is based on a thermal inertia parameter of $\gamma = 750$ cm^2 – sec$^{1/2}$ – °C/cal.

In order to determine the directionality of emission, the control area will be scanned from an observation angle of ω. The observed emission is

$$J_0 = \left(1 - \sum_{i=1}^{n} A_{Dn}\right)(S \sin\delta + q_s) \sin\omega + \sum_{i=1}^{n} \int_{A_n} J_{cn}(\mathbf{n} \cdot \mathbf{c}) dA_n \qquad (3)$$

where $\mathbf{n} \cdot \mathbf{c}$ is the scalar product of the crater surface unit normal vector and the unit vector in the direction of observation.

As shown in Fig. 1, part of the crater surface is not visible to the observer; consequently, the integration in Eq. (3) includes only the visible regions of the crater surfaces. As an example, Fig. 2 illustrates that in viewing an $a = 3$ aspect ratio crater, illuminated at a solar elevation angle of 10° and observing the crater surface in the lunar equatorial plane at an observation angle of ω, part of the crater is not visible. From the direction of the sun, part of the shadowed region is not visible. Viewing from the opposite side, almost all of the sunlit region is invisible. This geometrical phenomenon gives a simple explanation for the directionality of lunar surface emission.

In order to measure the directionality of emission, the average emission will be defined, normal to the flat surface as

$$J_n = J_0/\sin\omega \qquad (4)$$

From where the brightness temperature is

$$T = (J_n/\sigma)^{1/4} = (J_0/\sigma \sin\omega)^{1/4} \qquad (5)$$

In determining the brightness temperatures for various topographical conditions and solar and observation angles, Eq. (3) is evaluated first numerically, by using Eq. (2) for each of the craters. Then the brightness temperature can be obtained from Eq. (5). For the actual computations it is more practical to evaluate the two parts of Eq. (3) individually, normalize eaeh for unit surface area and "mix" the two parts according to the surface topography.

Discussion of Results

Figure 3a illustrates the brightness temperatures for subsolar conditions for $a = 4$ and $a = 3$ aspect ratio craters. (The area of the control surface, which is the area of opening of the crater, is unity.) The brightness temperature of the flat lunar surface is also illustrated ($a = \infty$) which is constant (assuming that the flat surface is Lambertian). At an observation angle of 0° from the zenith, the brightness temperature for an $a = 3$ aspect ratio crater is approximately 5° K highet than the brightness temperature of the lunar plain. This difference reduces rapidly with the increase of the aspect ratio. It is only around 2° K for an $a = 4$ aspect ratio crater. As

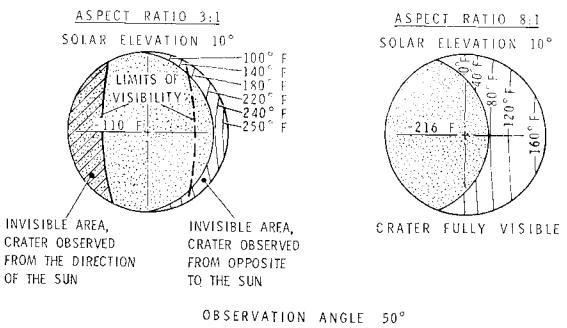

Fig. 2 Temperature distribution and visible regions of lunar craters.

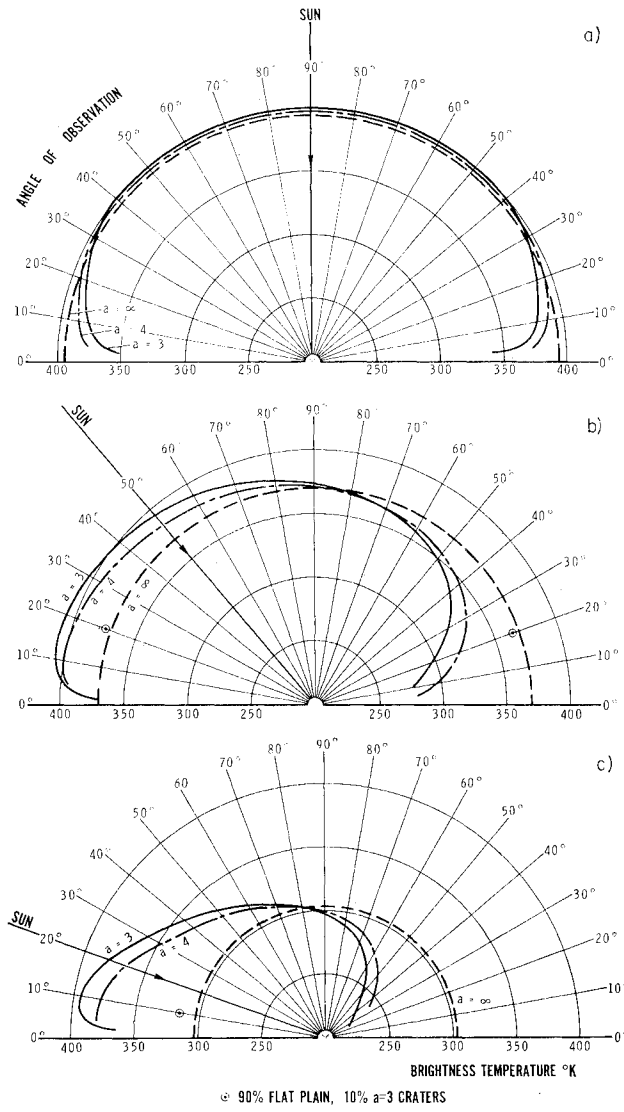

Fig. 3 Brightness temperatures at the lunar equator. 90°, 50°, and 20° solar elevation from horizon.

indicated in Fig. 3a a cratered lunar surface at subsolar conditions and at high observation angles (measured from the horizon) can be considered nearly Lamertian.

Figure 3b shows the directional behavior of brightness temperature for a 50° solar elevation (40° from zenith). The directionality is more pronounced here. It is interesting to note that the maximum of the brightness temperature is at a lower observation angle than the solar elevation angle. This behavior was also observed by Shorthill.[2] Furthermore, on the cool side, the crater with higher aspect ratio results in greater brightness temperature at low observation angles, despite the fact that the shadows of shallow craters are colder than those of deep craters. This apparent paradox can be explained by Fig. 2. By observing the shadowed side in a deep crater at a low observation angle, the warm region of the crater is not visible to the observer, while shallow craters are fully visible, including the sunlit region, which increases the average brightness temperature.

The directional behavior of the emission at 20° solar elevation is shown in Fig. 3c. The directionality is very pronounced, the maximum of the brightness temperature curve is lower than the solar elevation angle, especially at the higher aspect ratio crater, where it approaches the horizon. The point corresponding to the rough surface consisting of 90% flat plain and 10% $a = 3$ aspect ratio craters is also indicated on the hot side. The brightness temperature for such a surface is around 13° K higher than the brightness temperature of the Lamertian plan.

Figures 3a, b, and c well indicate that the lunar surface can be considered Lamertian at high solar elevation and observation angles. For low-solar elevation angles the surface deviates more and more from the Lambertian behavior. The present model is highly idealized, but a crater field still represents a reasonable approximation, as can be seen from the high resolution lunar photographs. Many of the lunar craters are flat bottomed and cannot be considered spherical. Such craters would increase the directionality even more at low-elevation angles.

In Fig. 4 the results of the present study are superimposed on the representation of experimental data given by Shorthill,[2] taken along the north and south sections of the lunar equator. The experimental data were approximated by two conditions, one is a $a = 7.5$ aspect ratio crater, the other is a mix of 10% $a = 3$, 20% $a = 4$, 30% $a = 7.5$ aspect ratio craters and 40% flat plain. Both of these hypothetical cases are in good agreement with the experimental data, both in magnitude and trend. In order to determine the directional behavior of the radiation in a particular region of the lunar surface, however, it is necessary to know the topography of that region.

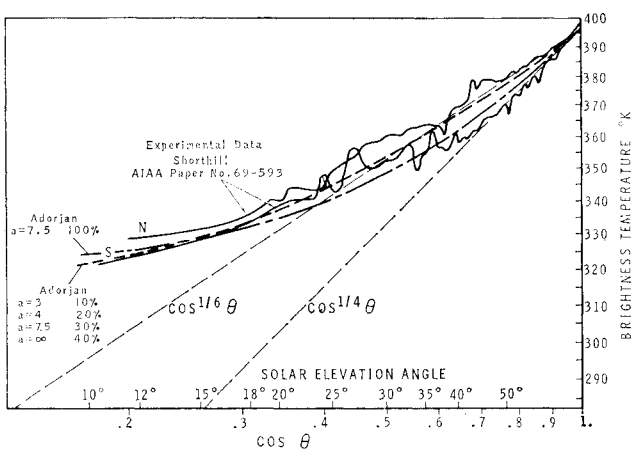

Fig. 4 Variation of brightness temperature of the full moon in north-south direction.

References

[1] Pettit, E., and Nicholson, B., "Lunar Radiation and Temperatures," *Astrophysical Journal*, Vol. 71, 1930, pp. 102–135.

[2] Shorthill, R. W., "The Infrared Moon," *Journal of Spacecraft and Rockets*, Vol. 7, No. 4, April 1970, pp. 385–397.

[3] Adorjan, A. S., "Temperature Distribution in Shadowed Lunar Craters," *Journal of Spacecraft and Rockets*, Vol. 7, No. 3, March 1970, pp. 378–380.

Exhaust Velocity Studies of a Solid Teflon Pulsed Plasma Thruster

KEITH I. THOMASSEN*
Massachusetts Institute of Technology, Cambridge, Mass.
AND
ROBERT J. VONDRA†
MIT, Lincoln Laboratory, Lexington, Mass.

Introduction

PULSED electric thrusters have proved to be useful for satellite control applications. We report here on a continuing diagnostics program on the solid Teflon fuel thrusters developed by Fairchild–Hiller[1] and used on the LES-6 satellite (Lincoln Experimental Satellites)[2,3]. The purpose of the program is to understand the physics of the discharge, develop mathematical models of the device to predict performance, and measure circuit and plasma parameters in order to improve the design and the efficiency of the thruster.

Our results to date have been summarized elsewhere.[4,5] Briefly, parameters for a simple RLC circuit model were determined and used to predict thruster efficiency and impulse bit. Langmuir probe and microwave interferometry determined plasma exhaust densities, a Faraday cup measurement of time-of-flight yielded exhaust ion velocities, and a thrust stand was built to measure impulse bit and specific impulse.

From the early results we found a mass averaged exhaust velocity $\bar{v} = 3000$ m/sec ($I_{SP} = 300$ sec), but a Faraday cup used to measure ion current yielded an ion velocity of 40,000 m/sec by a time-of-flight measurement. This prompted a more detailed investigation of the constituents in the exhaust, which we report here. We are interested in knowing the constituents in the exhaust and their velocities, first so that we might understand the plasma formation process better, and second in order to determine the kinetic energy in the exhaust. The latter determines the fraction of stored energy imparted to the exhaust while the former is important in considering the design changes which will improve this efficiency.

It is perhaps worthwhile to note that early estimates of the kinetic energy (2% of the initial stored energy) were in error because they assumed all components in the exhaust traveled at the mass-averaged velocity. On obtaining the Faraday cup measurements it was clear that the ionized portion of the exhaust was traveling much faster, hence that the total energy

Presented as Paper 71-194 at the AIAA 9th Aerospace Sciences Meeting, New York, January 25–27, 1971; Submitted March 1, 1971; revision received August 12, 1971. This work was sponsored by the Department of the Air Force.

Index category: Electric and Advanced Space Propulsion.

* Associate Professor, Electrical Engineering Department.

† Staff Member, Space Communications Division. Member AIAA.